LBL-10387 c. 2
UC-70

SECONDARY MINERALS FOUND IN CORES DC2 A1 AND DC2 A2 TAKEN FROM THE GRANDE RONDE BASALT FORMATION, PASCO BASIN, WASHINGTON

L. S. Teague

January 1980

Prepared for the U.S. Department of Energy
under Contract W-7405-ENG-48

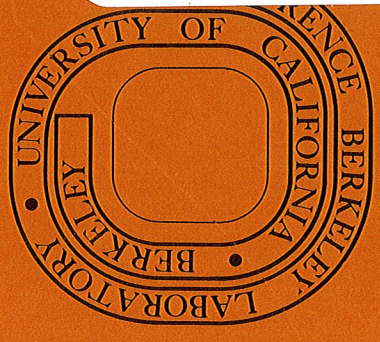

LBL-10387

SECONDARY MINERALS FOUND IN CORES DC2 A1 AND DC2 A2 TAKEN FROM THE GRANDE RONDE BASALT FORMATION, PASCO BASIN, WASHINGTON

L. S. Teague

Lawrence Berkeley Laboratory
University of California
Berkeley, CA 94720

Topical Report Number 1, Fiscal Year 1980
for Rockwell Hanford Operations of Rockwell
International under Contract MOA-SBB-202849

TABLE OF CONTENTS

LIST OF TABLES

LIST OF FIGURES

INTRODUCTION

The results obtained for Task I are presented and discussed in this report. The subject of Task I is the study and identification of secondary mineral assemblages in two slant cores drilled off core DC2. The data were obtained from scanning electron microscopic (SEM/EDAX), x-ray diffraction (XRD), and thin section petrographic studies. In addition, an attempt was made to determine the lateral continuity of the secondary mineralization and the extent to which the fissures in this potential repository horizon were interconnected.

SAMPLING PROCEDURES

Samples were obtained from two drill cores, DC2 A1 and DC2 A2, both of which were drilled at an approximately 30° slant from DC2. Figure 1 shows the location of DC2 and other drill cores previously studied. Figure 2 shows the vertical distribution of samples taken from the two slant cores and DC2. An attempt was made to obtain an even vertical distribution of samples; however, this was not completely successful because large intervals of core often lacked sufficient vesicles and fractures for adequate characterization. The samples are considered representative of the core intervals in which they occur.

To prevent any ambiguity in interpretation of the results, XRD and SEM samples were taken from the same vesicles or fractures. After the SEM/EDAX examination of a sample was completed, the same sample was sometimes used in the XRD studies. Thin sections were obtained from the same depths as the SEM and XRD samples.

The alphanumeric labeling system used by Benson, et al. (1979) was also used here. The identification number includes the core number, the true vertical depth in feet, the type of analysis (S = SEM, X = XRD, P = petrographic) and the type of sample (v = vesicle, f = fracture).

SCANNING ELECTRON MICROSCOPY (SEM)

Procedures

Samples approximately 1 cm in diameter were attached to aluminum studs by epoxy cement and were coated with gold. A few samples, particularly those containing a fibrous mineral, were coated with a 100-Å amorphous carbon layer before gold coating to improve resolution at high magnifications (> 5000 X). Unfortunately, in most instances resolution was not significantly improved. The samples were examined with an AMR 1000A SEM equipped with an energy dispersive x-ray analyzer (EDAX). A total of 39 slant core samples were studied, of which 12 were from fractures.

Mineral identification was accomplished by the combined use of semi-quantitative chemical analysis (EDAX) and morphological observations (SEM). Additonal information was obtained from supplementary XRD data of the same vesicle or fracture samples. SEM observations of zeolite morphologies made by Mumpton and Ormsby (1978) and Sheppard (1976) aided in the identification of clinoptilolite and mordenite. Work by Finkleman (1975) and Klasik (1975) aided in the recognition of silica phases.

Results

Crystallization Sequences

Table 1 lists the crystallization sequences in samples from DC2 A1 and DC2 A2 observed with the SEM. Separate layers were distinguished on the basis of morphological and/or chemical differences. In some samples morphologically distinct layers had similar chemical compositions (e.g., DC2 A2 2690 S2, Figure 3). Intergrowths of two or more minerals were fairly common (DC2 A2 2960 S1 in Figure 3 illustrates an example of such intergrowth).

as well as other samples, XRD studies indicate the presence of more than one silica polymorph even though only one crystal habit was observed with the SEM. However, it is possible that additional, morphologically distinct silica phases are present but were covered by later minerals and not exposed in the sampling process. Partial inversion of a metastable silica phase also may have occurred in these samples. Van Valkenburg and Buie (1945) described silica octahedrons found in basalt vesicles from the Deccan volcanics in India. Using optical and x-ray means, they found that certain of the octahedrons were cristobalite while others were quartz. They concluded that some of the octahedrons had inverted to quartz while the others had remained cristobalite.

Both silica and clay often occur in more than one generation which were distinguished by different morphologies or separated by another mineral phase. In contrast, clinoptilolite apparently precipitated at only one stage in the crystallization sequence. Figure 4 shows typical clinoptilolite crystals. Mordenite (Figure 5) occurs as fibrous masses and is among the last minerals found to precipitate. Isolated fibers also were found which are probably mordenite but were not present in sufficient quantity to be positively identified by XRD. Euhedral pyrite crystals exhibiting a step-like growth pattern are shown in Figure 6. A hexagonal mineral high in abundances of calcium and phosphorus (Figure 6), tentatively identified as apatite, was found in two SEM samples.

Mineralogical Changes with Depth

The data in Table 1 seem to indicate an increase in the complexity of mineral sequences with depth. Samples from the lowest depths in each of the slant cores contain four or five minerals and sometimes multiple generations of silica or clay. This effect was not observed in core DC 2.

Clay, silica and clinoptilolite occur throughout the depth intervals sampled in DC2 A1 and DC2 A2. Mordenite was previously reported at depths below 900 meters (Benson, et al., 1979). This observation is compatible with abundant mordenite found in samples below 950 m in DC2 A1 and below 1000 m in DC2 A2.

Evidence of Dissolution

Only three samples from the slant cores exhibit signs of dissolution. Clinoptilolite was the only mineral containing such etch pits. The paucity of dissolution evidence may be due to the relatively small number of samples examined in this study.

Discussion of SEM/EDAX Results

Results of the slant core studies are similar to results from studies of DC2, DC6 and DH5. A generalized crystallization sequence for both fractures and vesicles in these cores is: clay (usually smectite) -> clinoptilolite -> silica/clay. Variations in this sequence commonly occur and layers may be skipped or additional minerals or mineral generations may be present. Differences between the cores appear to be minor and may be the result of the vertical distribution of the samples. The majority of the slant core samples are from the Umtanum flow and below while most of the DC2 samples are from above the Umtanum Unit (Figure 2). These differences are discussed below.

Table 2 shows mineral abundances for DC2 A1, DC2 A2 and DC2 obtained from the SEM data. Clay, clinoptilolite and silica are the most common minerals. Mordenite occurs with approximately the same frequency in the slant cores but is less abundant in DC2. Pyrite usually occurs in the fractures of DC2 while in the slant cores it is usually found in vesicles. Apatite is found only in vesicles in DC2 A2 and DC2.

Fracture mineralogy was found to be simpler in terms of number of mineral generations than vesicle mineralogy in all cores. Clay, silica, clinoptilolite and pyrite comprise the majority of minerals found in fractures. Apatite, mordenite and a few unidentified minerals were found in vesicles only. There appears to be an increase in the complexity of the crystallization sequences with depth in the slant cores but not in DC2. This difference between cores may be due to the lack of abundant data in the deeper portion of DC2. In the history of a particular basalt layer, this layer moves down section as later flows are deposited over it. Presumably, as the layer is covered with later flows it passes through different diagenetic environments in which additional secondary minerals are precipitated. Therefore, deeper samples reflect a longer diagenetic history, and hence, contain a wider variety of secondary minerals. This effect can be observed if secondary minerals remain intact thereby preserving a record of their formation. Both the mordenite and dissolution data from the slant cores are too sparse to conclusively determine their depth dependence.

Based on the overall similarity of all drill cores (slant and vertical), we have formed the preliminary conclusion that the secondary mineralization is laterally continuous. Clay, clinoptilolite and silica are common and found throughout all the drill cores studied by this group. However, the data of Ames (1976) indicate that clinoptilolite is absent from the mineral assemblage above a depth of 400 m. Similarities in mineral morphologies and crystallization sequences are also common. The extent to which the fractures are interconnected cannot be determined from the data given here. Although the similarity of the secondary minerals througout the cores may indicate that the fractures are or were connected, this is not necessarily true. Migration of fluids through the basalt could occur by a number of means: (1) through

interconnected vesicles, (2) through interconnected fractures, or (3) through micropores in the rock itself. Most vesicles do not appear to be connected; infrequently, solution-enlarged vesicles are found which formed near the top of gas-rich flows. There is no definite evidence from this study regarding fracture connectivity because the data and observations are primarily one-dimensional. Thin sections do not reveal any microfracture systems. Due to the lack of definite evidence for the interconnection of fractures and vesicles, migration through micropores within the basalt remains a possible means of fluid and mass transport.

X-RAY DIFFRACTION (XRD) STUDIES

Procedures

XRD samples were ground to a fine powder, mixed with a silicon standard and applied to a glass slide with balsam dissolved in xylene. The powders were analyzed with Ni-filtered Cu Kα radiation (λ = 1.54 Å) using a Norelco diffractometer equipped with a graphite monochromater. The resulting diffraction patterns were indexed using ASTM cards and computer-generated patterns made from the ASTM data. Only those XRD samples whose corresponding SEM samples had some mineral of interest were analyzed; all samples containing a fibrous or unknown mineral were examined by x-ray diffraction.

Mineral abundances were estimated by calculating integrated intensities using the height and half-width of the most intense peak for each mineral. However, it should be noted that these estimates are only semi-quantitative because entire vesicle or fracture fillings were not sampled.

Results

Figure 7 shows x-ray diffraction patterns for some of the commonly occurring secondary minerals. The top pattern shows the reflections for the

fibrous zeolite, mordenite. DC2 A1 3245 x1, shows the peaks for quartz, cristobalite and smectite. The large broad peak in the second and third patterns centered around 16 degrees (2θ) is from the mounting medium. DC2 A2 2960 x3 contains three silica phases (quartz, cristobalite and tridymite), clinoptilolite, and smectite. The broadness at the base of the group of peaks around 22 degrees (2θ) may be from opal but could also result from the overlapping of these peaks. DC2 A1 3020 x2 shows the pattern for an atypical clinoptilolite in which the peak at approximately 4.0 Å (23 degrees, 2θ) is larger than that at 9.0 Å (10 degrees, 2θ). All of the other clinoptilolites in these samples show the reverse relationship between these two reflections. However, this variation cannot be used to characterize particular clinoptilolites because these differences are minor. In addition, the diffraction patterns of the clinoptilolites and their isomorphous counterpart, heulandite, are generally simlar and the XRD analyses do not conclusively identify the end member.

Eighteen XRD samples were analyzed. Table 3 lists the XRD analyses for DC2 A1 and DC2 A2. These data also have been incorporated in the SEM/EDAX data in Table 1.

Discussion of XRD Results

XRD data in this report were used exclusively to supplement the SEM/EDAX information. The tentative identification of the fibrous mineral seen in the SEM samples (Figure 5) as mordenite was confirmed by x-ray diffraciton. Several silica phases were found, sometimes several in one sample. As previously mentioned, these were often associated with only a single silica morphology. Opal occurs in the slant cores but is absent in DC2. This variation is probably due to differences in the vertical distribution of the samples.

THIN SECTION PETROGRAPHY

Procedures

A thin section was prepared for each depth studied with the SEM. Most sections contained more than one vesicle or fracture. Eleven vesicles and 12 fractures were examined and point counted using a standard petrographic microscope. The zeolite and silica phases generally occurred as optically similar, fine-grained material and were difficult to differentiate. Supplementary SEM/EDAX and XRD data clarified the identification in some samples, but many minerals remain unidentified. These mineral identifications have been incorporated in Table 4.

Results

Figure 8 shows several examples of the secondary minerals examined and Table 4 lists the observed crystallization sequences. An initial brown to orange-brown clay is present in all fractures and vesicles. In two samples, the initial clay is intergrown with another mineral: once with clinoptilolite and once with a green clay. Clinoptilolite was identified by its euhedral lath-like to tabular crystals resembling, in two dimensions, its form in the SEM samples. Clinoptilolite is the most common second-formed phase, occurring 59 percent of the time. The second-formed phase is silica 18 percent, clay 12 percent and an unidentified zeolite 12 percent of the time. In the samples containing both clinoptilolite and silica, clinoptilolite always formed before silica. Clay is the third-formed phase 50 percent of the time. Other third-formed phases are: an unknown mineral (29 percent), silica (14 percent) and mordenite (7 percent).

Point counting of the secondary minerals (Table 5) shows the predominance of brown clay, clinoptilolite and silica. Note that vesicles and fractures from the same depths have widely varying amounts of secondary minerals.

Discusion of Petrographic Data

The petrographic data support the results of the SEM/EDAX studies. Although crystallization sequences can be obtained more easily from thin section, the lack of chemical data presents a problem in distinguishing zeolites and silica. Supplementary XRD and SEM data aid in the identification of some, but not all, the unknown minerals. In all samples containing an unknown mineral, clinoptilolite was found. Since data from the SEM indicate clinoptilolite occurs only in a single generation, the unknown mineral is probably a silica phase. However, it is possible that the unknown mineral is mordenite although mordenite usually has a more fibrous habit. Point counting results indicate the wide variation in the volumes of the minerals. These variations exist over the space of a few centimeters and are probably due to local differences in void size and fluid and basalt compositions.

SUMMARY AND CONCLUSIONS

One purpose of this study was the characterization of the secondary mineral assemblages in two slant cores and the comparison of this data with that previously obtained from the associated vertical core, DC2. The SEM, XRD and petrographic data for the slant cores are similar to those of the vertical cores, DC2, DC6, and DH5. The generalized crystallization sequence is: clay (usually smectite) -> clinoptilolite -> silica and/or clay. Both clay and silica often formed in one or more generations and many other variations upon the basic sequence were observed. Some vesicles and fractures are missing the latter portion of the sequence, probably as a result of voids becoming filled at an early stage in the diagenetic evolution of the basalts. Fractures, with less void space than

the vesicles, may have been isolated from the circulating fluids earlier in the sequence than the vesicles. This would account for the simpler mineralogy found in the fractures since minerals other than clay, silica and clinoptilolite generally formed late in the sequence. Other variations might have been caused by the isolation of the vug or fracture from the advective system during different periods of precipitation or by local compositional variations in the fluid-basalt system.

Differences between the slant cores and DC2 may be due to variations in the vertical distribution of the samples and the fewer slant core samples studied. As a result, firm conclusions cannot be drawn regarding the depth dependence and relationship of mordenite precipitatiopn to clinoptilolite dissolution.

The limited data obtained in this and previous reports supports the preliminary conclusion that secondary mineralization is laterally continuous. Secondary mineral assemblages and morphologies in all cores are similar and no significant horizontal changes are observed. Early in the diagenetic history of the basalts, interflow fluid and chemical transport may have occurred principally along fractures. After the fractures became more or less filled with secondary minerals, a significant portion of the transport may have occurred and may be occurring via networks of micropores.

REFERENCES

1. Ames, L. L., 1976. Hanford basalt flow mineralogy. An unpublished report to the Rockwell Hanford Operations Office of North American Rockwell.

2. Benson, L. V., L. S. Teague, C. A. Mouton, C. J. Frisch, R. A. Stolzman and D. J. Corrigan, 1979. A study of rock-water-nuclear waste interactions in the Pasco Basin, Washington, Part I: Distribution and compositon of secondary and primary mineral phases in basalts of the Pasco Basin, LBL-9677.

3. Finkleman, R. B., 1975. Perched silia minerals on mordenite fibers. Jour. Research U. S. Geol. Survey, 3, 197-202.

4. Klasik, J. A., 1975. High cristobalite and high tridymite in Middle Eocene deep-sea chert, Sci., 189, 631-632.

5. Mumpton, F. A., and W. C. Ormsby, 1978. Morphology of zeolites in sedimentary rocks by scanning electron microscopy. In Natural Zeolites Occurrence, Properties, Use, edited by L. B. Sand and F. A. Mumpton, New York, Pergamon Press, 113-134.

6. Sheppard, R. A., 1976. Zeolites in sedimentary deposits of the northwestern United States - potential industrial materials. Montana Bureau of Mines and Geology Spec. Pub. 74, 69-84.

7. Van Valkenburg, A., Jr., and B. F. Buie, 1945. Octahedral cristobalite with quartz paramorphs from Ellora Caves, Hyderabad State, India Am. Min., 30, 526-535.

TABLES

TABLE 1

SEM/EDAX DATA FOR DC2 A1 AND DC2 A2

Sample	Depth (m)	Crystallization Sequence	Comments
DC2 A1 2394 S1 (v)	730	C -> Si -> Cl	
S2 (f)		S -> Q	
S3 (v)		C -> Si -> Cl -> Si	
DC2 A1 3020 S1 (v)	920	Cl -> Q	
S2 (v)		Cl -> Fi -> C	
S3 (f)		Cl	
DC2 A1 3084 S1 (f)	941	Cl	
S2 (f)		Cl -> Si	
S3 (v)		Cl -> Si	
DC2 A1 3194 S1 (v)	974	Cl -> M	
S2 (v)		Cl -> Cl -> C -> Cl	Diss
S3 (v)		Cl -> C -> Cl -> Q	Diss
DC2 A1 3245 S1 (f)	989	S -> Q/CR	
S2 (v)		Cl -> Si	
S3 (v)		Cl -> Cl (Ca) -> Cl	
DC2 A1 3282 S1 (v)	1000	S -> C -> CR -> M - Cl - Py -> Cl	
S2 (v)		Cl -> C -> CR/Op -> CR/Op -Cl - M(?)	
S3 (v)		S(?) -> C -> Cl - Cl (Fe)	
S4 (v)		S(?) -> Cl -> C -> Cl - Cl (Mg)	
DC2 A2 2690 S1 (v)	820	Cl -> KNa	
S2 (v)		Cl	
S3 (f)		Cl -> C	
DC2 A2 2960 S1 (v)	902	Cl -> C -> Si - Ap (?) - Cl -> Fi	
S2 (f)		Cl -> C	
S3 (f)		S -> CR/T/Q	
DC2 A2 3024 S1 (v)	922	C -> Cl	
S2 (v)		Cl -> Si	
S3 (f)		Si - Cl	
DC2 A2 3153 S1 (v)	961	Cl -> Q	
S2 (v)		Cl -> Q(?)	
S3 (f)		Cl -> C -> Si	
DC2 A2 3234 S1 (v)	986	Cl	
S2 (f)		Cl	
S3 (v)		S -> Q/Op	

TABLE 1 (Cont.)

SEM/EDAX DATA FOR DC2 A1 AND DC2 A2

Sample	Depth (m)	Crystallization Sequence	Comments
DC2 A2 3314 S1 (v)	1010	I -> C -> Op/CR/T -> M	
S2 (v)		Cl -> C -> Py -> Si -> M (?)	
S3 (v)		Cl -> C -> Q -> M	Diss
S4 (v)		Cl -> C -> Py -> CR/T -> Ap(?)-Si	
S5 (f)		Cl -> Py	

Legend

Ap	=	apatite
C	=	clinoptilolite
Cl	=	clay. Distinctive or especially abundant components listed in parentheses.
CR	=	low-cristobalite
Diss	=	dissolution in clinoptilolite was observed.
Fi	=	fibrous mineral
H	=	heulandite
I	=	iron-illite (celadonite)
K	=	potassium aluminum silicate
KCa	=	potassium calcium aluminum silicate
KNa	=	potassium sodium aluminum silicate
M	=	mordenite
Op	=	opal
Py	=	pyrite
Q	=	low-quartz
S	=	smectite
Si	=	silica
T	=	tridymite
v	=	vesicle
f	=	fracture
?	=	tentative identification. Based on chemical and morphological characteristics or comparisons with samples at same depth in the core.
/	=	separates phases identified with XRD which cannot be correlated with different morphologies.
-	=	separates phases which are intergrown.

TABLE 2

PERCENT OF FRACTURE AND VESICLE SAMPLES
CONTAINING A SPECIFIC SECONDARY MINERAL
DETERMINED BY SEM/EDAX

Secondary Mineral	FRACTURE SAMPLES				VESICLE SAMPLES			
	DC2 A1	DC2 A2	Σ*	DC2	DC2 A1	DC2 A2	Σ	DC2
Silica	60	43	50	60	57	69	63	48
Clinoptilolite	0	43	25	0	57	46	52	47
Clay	100	100	100	83	100	100	100	87
Mordenite	0	0	0	0	21	31	26	6
Pyrite	0	14	8	17	7	15	11	0
Apatite	0	0	0	0	0	15	7	2

*Σ indicates average for DC2 A1 and DC2 A2

TABLE 3

X-RAY DIFFRACTION DATA FOR DC2 A1 AND DC2 A2

Sample Number	Depth (m)	S	I	Q	CR	T	Op	C	M	H
DC2 A1 2394 x2' (f)	730			d						
x2" (f)		d								
DC2 A1 3020 x1 (v)	920			d						
x2 (v)								d		
DC2 A1 3194 x1 (v)	974								d	
x3' (v)				d						
DC2 A1 3245 x1 (f)	989	m		d	m					
DC2 A1 3282 x1 (v)	1000	a							m	
x1' (v)					t				d	
x2 (v)					d		m			
P2* (v)				d	m					
DC2 A2 2960 x3 (f)	902	m		t	d	m		m		
DC2 A2 3153 x1 (v)	961			d						
DC2 A2 3234 x3 (v)	986	m		d			t			
DC2 A2 3314 x1' (v)	1010				a	m	a	m		
x1" (v)			m					m	d	
x3 (v)				t				d	a	
x4 (v)					d	a	a	m		

LEGEND

v = vesicle
f = fracture

d = dominant
a = abundant >20%
m = minor 6 - 20%
t = trace 1 - 5%

C = clinoptilolite
CR = low-cristobalite
H = heulandite
I = iron-illite (celadonite)
M = mordenite
Op = opal
Q = low-quartz
S = smectite
T = tridymite

*XRD sample from thin section chip

TABLE 4

CRYSTALLIZATION ORDER IN DC2 A1 AND DC2 A2
DETERMINED BY THIN SECTION PETROGRAPHY

Sample Number	Depth (m)	Crystallization Sequence
DC2 A1 2394 P1 (v)	730	C1 -> C -> u (sph) -> C1
P2 (f)		C1 -> C -> u (rad)
P3 (f)		C1
DC2 A1 3020 P1 (f)	920	C1 -> C -> u (rad)
P2 (v)		C1 - C -> Si (?)
DC2 A1 3088 P1 (f)	941	C1 -> C -> C1 -> u (sph) -> Si
DC2 A1 3194 P1 (v)	974	C1 -> C1 (gr) -> M (?) -> C1
P2 (v)		C1 -> C1 (gr) -> C1 -> C -> C1 (gr)-C1
P3 (f)		C1 - C1 (gr)
DC2 A1 3245 P1 (f)	989	S -> Q/CR
P2 (v)		C1 -> Si
DC2 A1 3282 P1 (f)	1000	C1
P2 (v)		C1 -> C -> C1 -> Q/CR -> z (fib)
P3 (v)		C1 -> C -> C1
DC2 A2 2690 P1 (f)	820	C1 -> C -> u (rad) -> C1
P2 (v)		C1
DC2 A2 2960 P1 (f)	902	S(?) -> C -> CR/T/Q(?)
DC2 A2 3024 P1 (f)	922	C1 -> C
P2 (v)		C1 -> z -> C1
DC2 A2 3153 P1 (f)	961	C1 -> C -> C1 -> u (rad)
DC2 A2 3234 P1 (f)	986	C1 -> Si
P2 (v)		C1
DC2 A2 3314 P1 (v)	1010	C1 -> z -> C1 - C -> Si

TABLE 4 (Cont.)

CRYSTALLIZATION ORDER IN DC2 A1 AND DC2 A2
DETERMINED FROM THIN SECTION PETROGRAPHY

Legend

C	=	clinoptilolite
Cl	=	clay. Brown unless otherwise noted
CR	=	low-cristobalite
fib	=	fibrous
gr	=	green
M	=	mordenite
Op	=	opal
Q	=	low-quartz
rad	=	radiating crystals (under crossed polars)
S	=	smectite
Si	=	silica
sph	=	speroidal
T	=	tridymite
u	=	unknown mineral, probably silica or zeolite
z	=	zeolite, specific type unknown
v	=	vesicle
f	=	fracture
?	=	tentative identification based on comparison of SEM, XRD and/or optical characteristics of similar minerals.
/	=	separates phases identified with XRD but exhibiting a single morphology
-	=	separates phases which are intergrown

Note: Mineral identification of all phases (except C) was based on XRD data.

TABLE 5

ESTIMATES OF RELATIVE AMOUNTS OF SECONDARY MINERALS IN FRACTURES AND VESICLES OF DC2 A1 AND DC2 A2 FROM POINT COUNTING

Sample Number	Depth (m)	Green clay	Brown clay	Clinoptilolite	Mordenite(?)	Silica (All phases)	Unknown Zeolite	Unknown
DC2 A1 2394 P1(v)	730		30	58				12
P2(f)			13	53				34
P3(f)			100					
DC2 A1 3020 P1(f)	920		32	54				14
P2(v)			13	15		72		
DC2 A1 3088 P1(f)	941		44	24		9		23
DC2 A1 3194 P1(v)	974	9	14		77			
P2(v)		18	61	21				
P3(f)		24	76					
DC2 A1 3245 P1(f)	989		18			82		
P2(v)			44			56		
DC2 A1 3382 P1(f)	1000		100					
P2(v)			9	4		6	81	
P3(v)			44	56				
DC2 A2 2690 P1(f)	820		9	53				38
P2(v)			100					
DC2 A2 2960 P1(f)	902		79	13		8		
DC2 A2 3024 P1(f)	922		56	44				
P2(v)			41				59	
DC2 A2 3153 P1(f)	961		62	15				23
DC2 A2 3234 P1(f)	986		76			24		
P2(v)			100					
DC2 A2 3314 P1(v)	1010		13	12		62	13	

LEGEND

v = vesicle
f = fracture
? = presence not confirmed by XRD

FIGURES

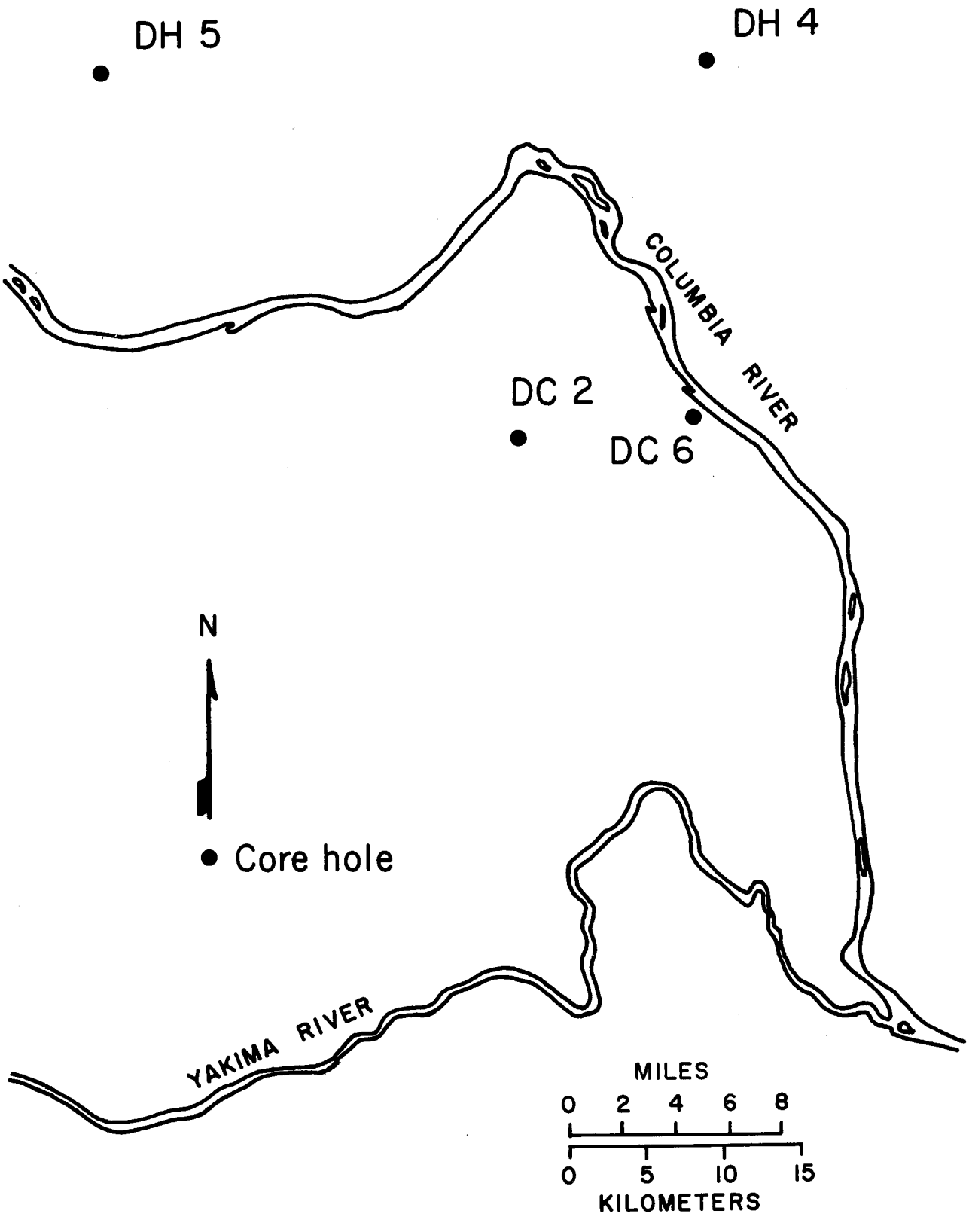

XBL 796-7541

Figure 1

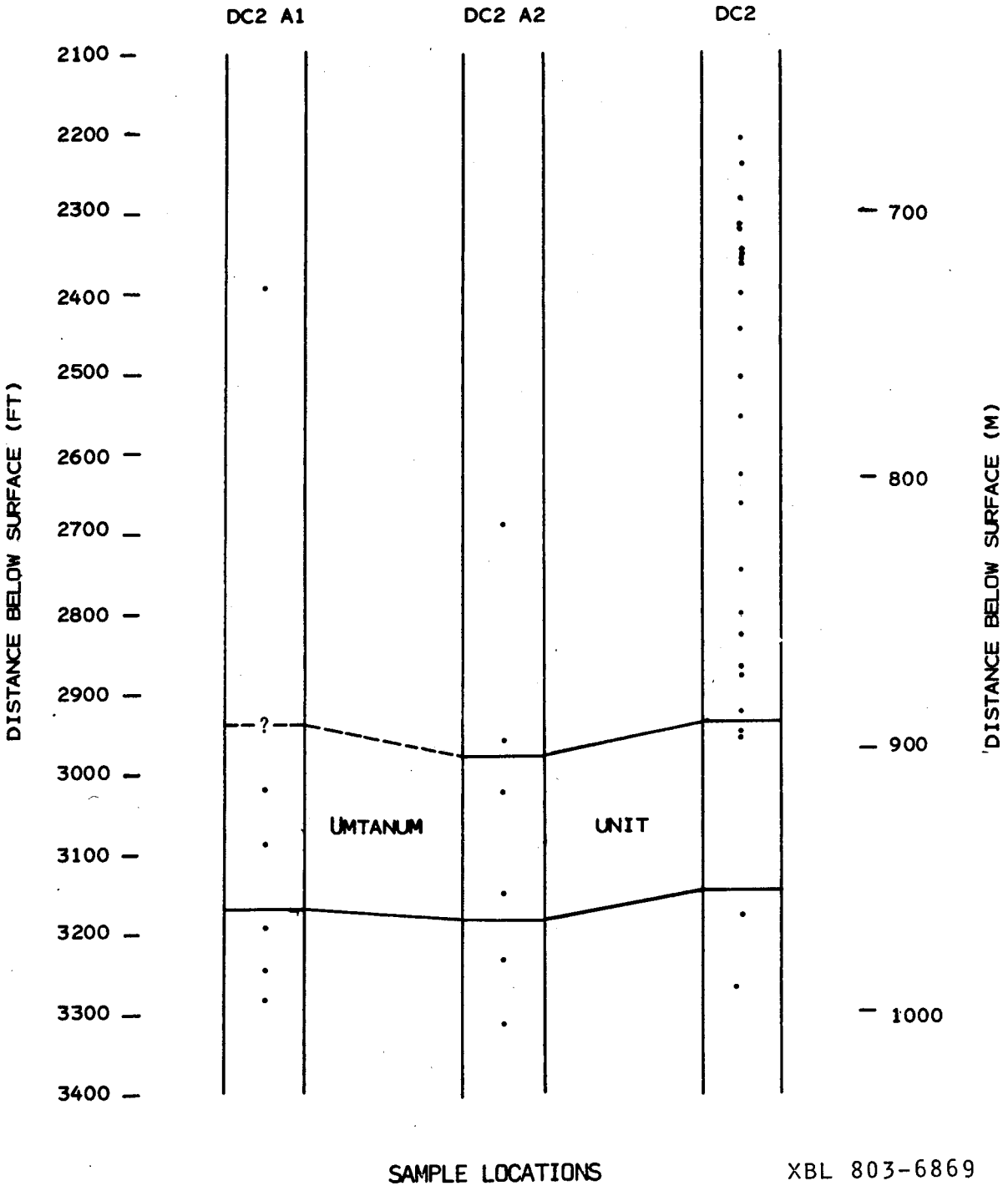
DC2 A1
DC2 A2
DC2
2100
2200
2300
2400
2500
2600
2700
2800
2900
3000
3100
3200
3300
3400
DISTANCE BELOW SURFACE (FT)
700
800
900
1000
DISTANCE BELOW SURFACE (M)
?
UMTANUM
UNIT
SAMPLE LOCATIONS
XBL 803-6869

FIGURE 2

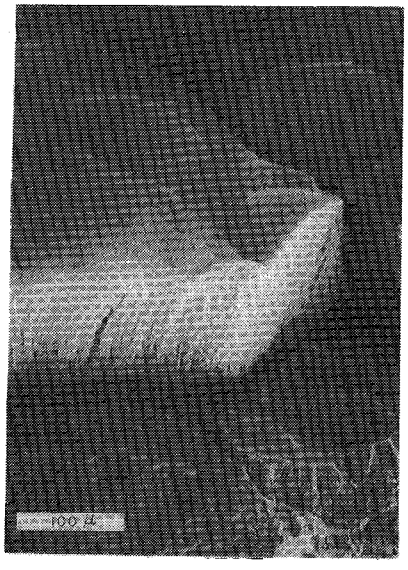

DC2 A2 2690 S2

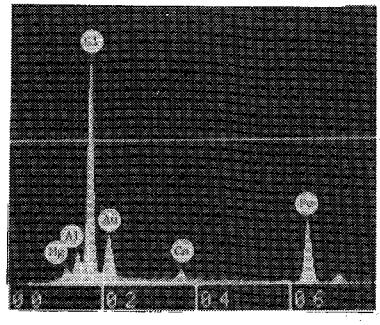

DC2 A2 2690 S2

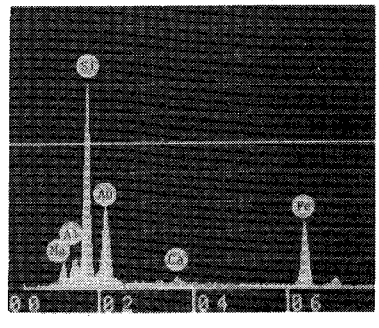

DC2 A1 3194 S3

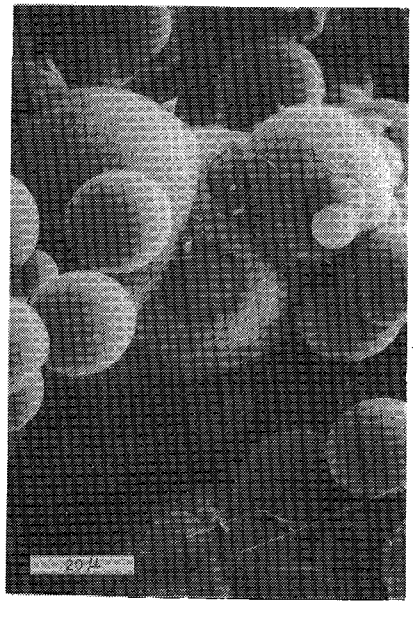

DC2 A2 2960 S1

DC2 A1 3194 S3

Figure 3

XBB 801-294

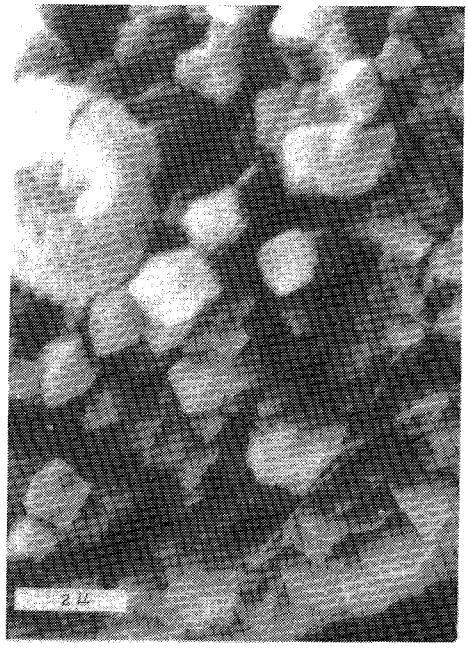

DC2 A1 3282 S2

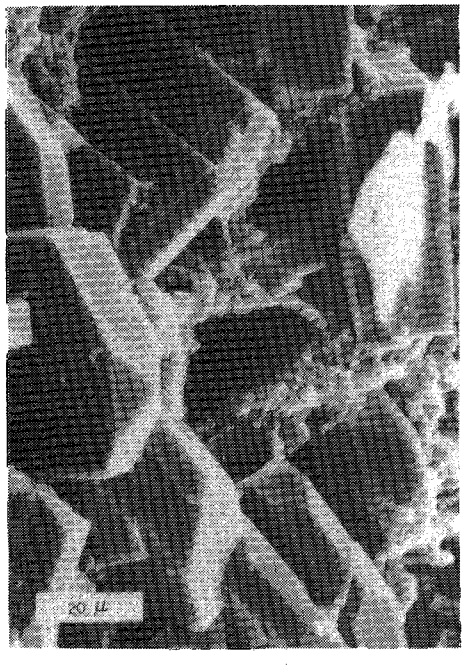

DC2 A1 3282 S4

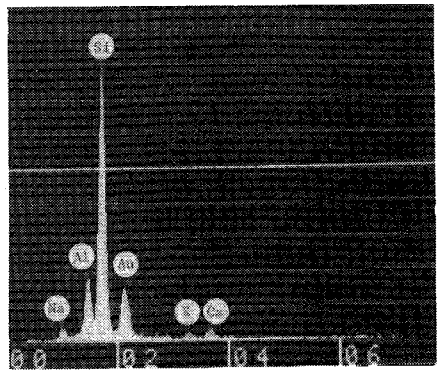

DC2 A1 3282 S4

Figure 4

XBB 801-298

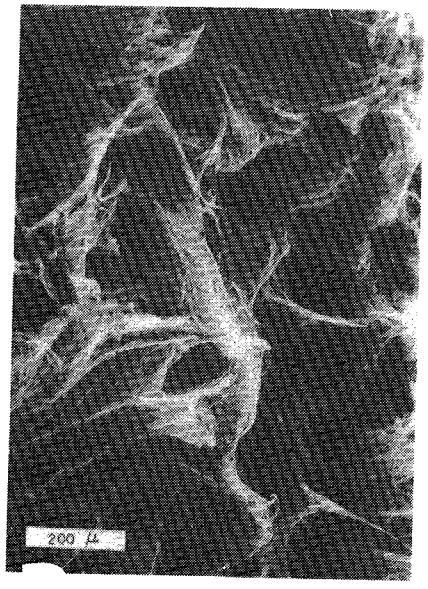

DC2 A2 3314 S1

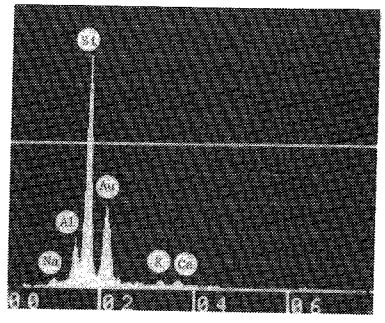

DC2 A2 3314 S1

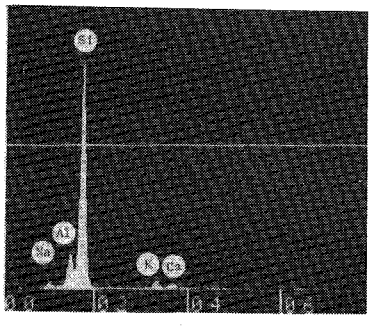

DC2 A2 3314 S3

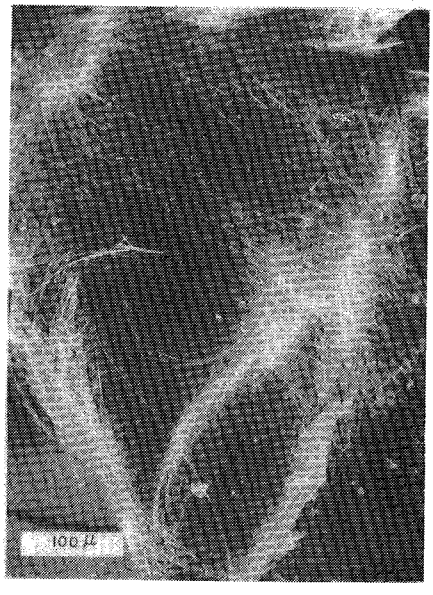

DC2 A2 3314 S3

Figure 5

XBB 801-297

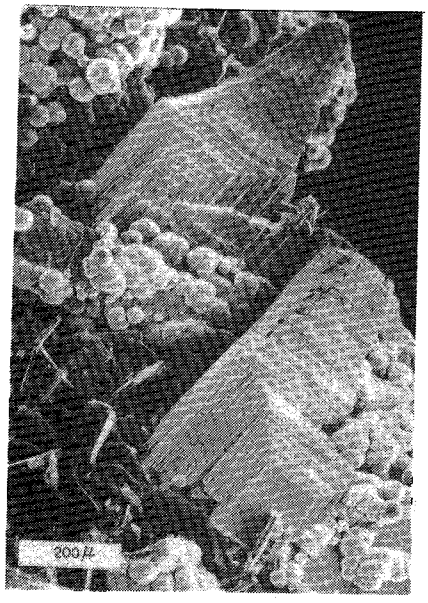

DC2 A2 3314 S2

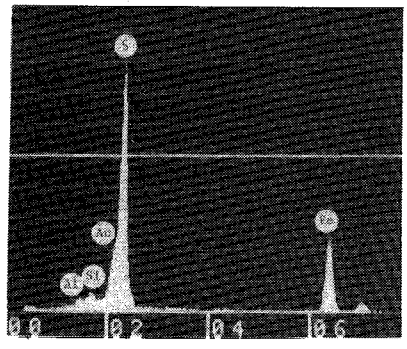

DC2 A2 3314 S2

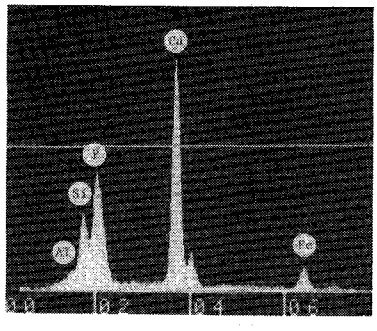

DC2 A2 2960 S1

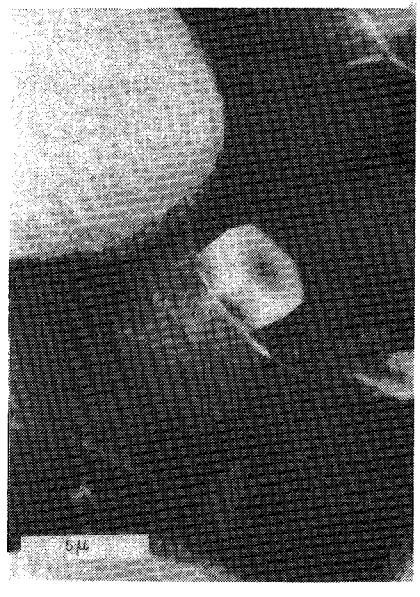

DC2 A2 2960 S1

Figure 6

XBB 801-296

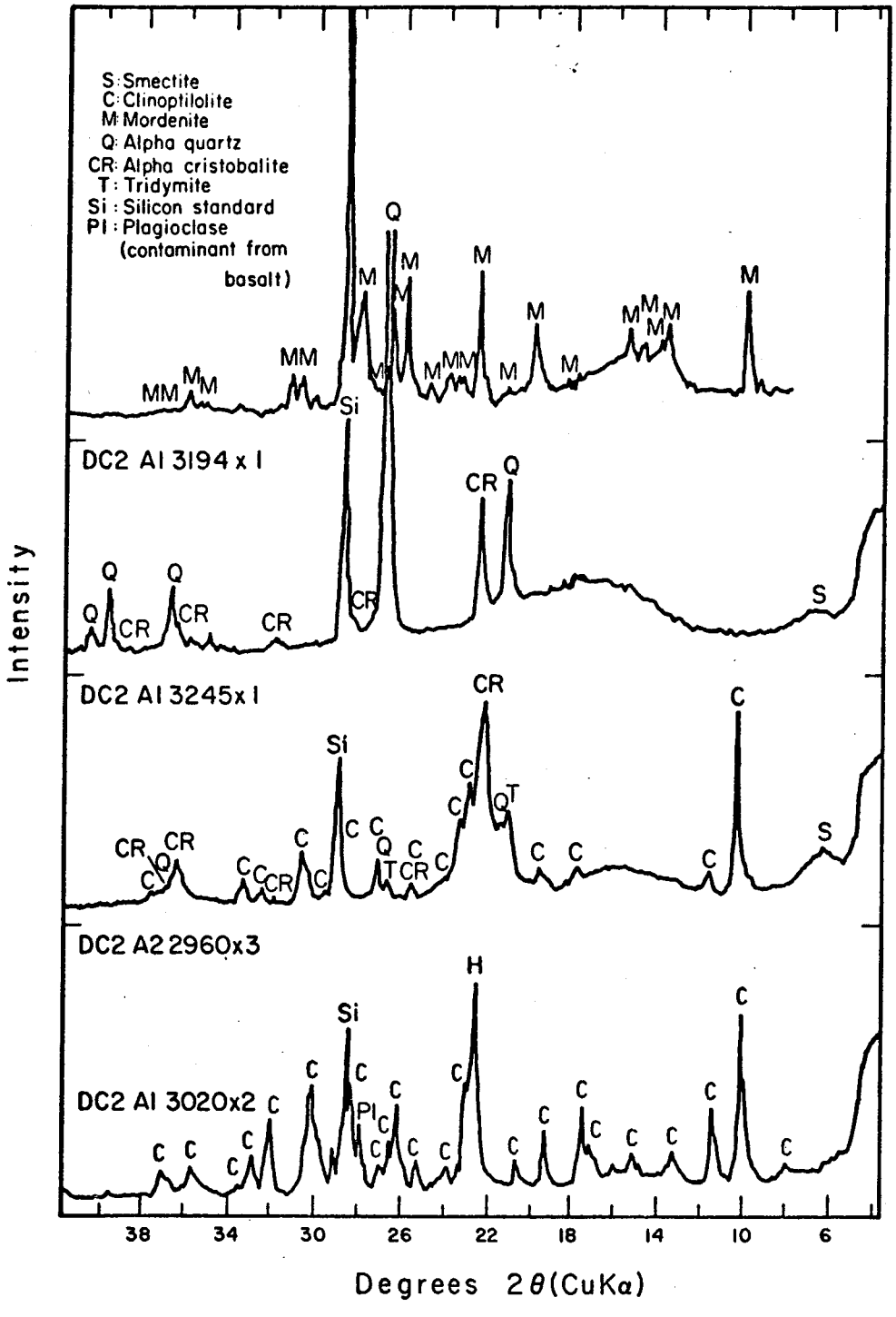

Figure 7
XBL 801-41

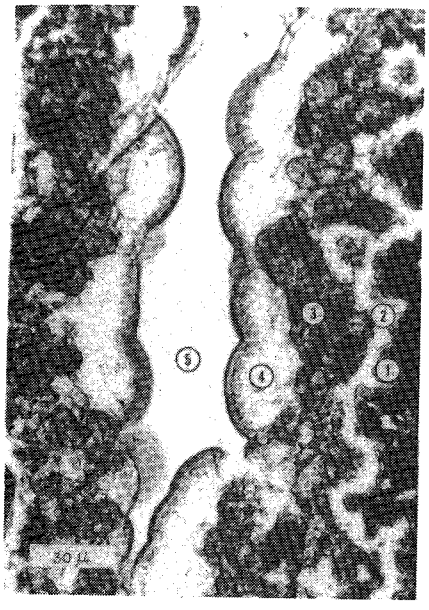

DC2 A1 3088 P1

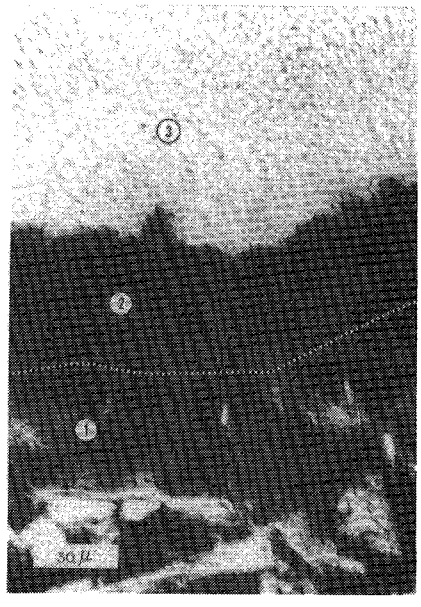

DC2 A1 3194 P1

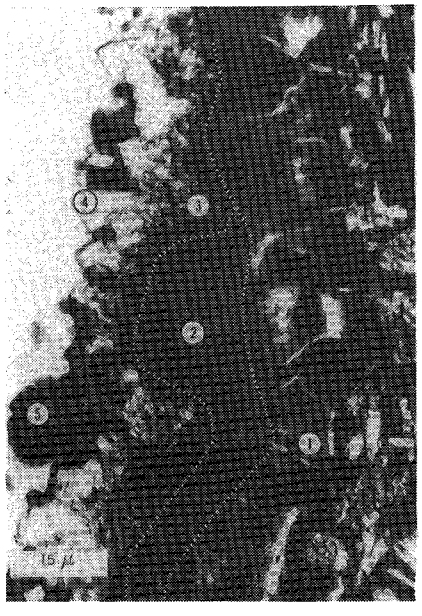

DC2 A1 3194 P2

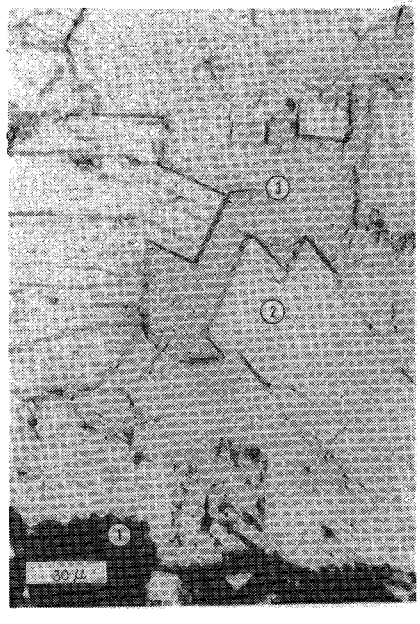

DC2 A2 2690 P1

Figure 8

XBB 801-295